2022-01-01

Validity of small-scale yielding regime in notched-cracked geometries

Borges, MF

10.1016/j.ijfatigue.2021.106563
International Journal of Fatigue

Validity of small-scale yielding regime in notched geometries

MF Borges[1], FV Antunes[1], DM Neto[1], JM Vasco-Olmo[2], FA Díaz[2], MN James[3, 4]

[1] *Univ Coimbra, Centre for Mechanical Engineering, Materials and Processes (CEMMPRE), Department of Mechanical Engineering*
[2] *Departamento de Ingeniería Mecánica y Minera, University of Jaén, Jaén, Spain.*
[3] *School of Engineering, Computing and Mathematics,University of Plymouth, Plymouth, United Kingdom.*
[4] *eNtsa, Nelson Mandela University, Port Elizabeth, South Africa.*

micaelfriasborges@outlook.pt
fernando.ventura@dem.uc.pt, http://orcid.org/0000-0002-0336-4729
diogo.neto@dem.uc.pt, https://orcid.org/0000-0002-2296-4009
fdiaz@ujaen.es
jvasco@ujaen.es
mjames@plymouth.ac.uk

ABSTRACT. The stress intensity factor range, ΔK, is widely used to study fatigue crack growth rate (FCGR), but its validity is not usually checked. This paper proposes a procedure based on crack tip opening displacement (CTOD) to define the boundary of the small-scale yielding (SSY) regime. In this approach, the elastic CTOD must be greater than 75% of the total CTOD in order to have SSY conditions. Numerical modelling was applied to notched samples with different notch radii, under both plane stress and plane strain conditions, with and without crack flank contact. Results indicate that an increase in notch radius promotes an increase of $\%\Delta\delta_e$, i.e. in the validity of SSY. In unnotched specimens, an increase in crack length promotes a progressive decrease of $\%\Delta\delta_e$. This effect of crack length is much more pronounced in notched specimens due to the local stress field concentration. Different alloys also show a significant yield strength effect with AA7050-T6 less prone to SSY than AA6082-T6, which is explained by its greater yield stress. Most of the situations studied fall outside the SSY regime, which reinforces the importance of verifying the applicability of LEFM to fatigue crack growth rate calculations.

KEYWORDS: FATIGUE CRACK GROWTH RATE; CTOD; SSY REGIME; NOTCH

INTRODUCTION

The stress intensity factor range, ΔK, is widely used as the crack driving force to characterise fatigue crack growth rate (FCGR). Different analytical models [1-3] have been proposed that relate crack propagation rate (da/dN) with this linear elastic parameter since it was first proposed by Paris and Erdogan [4] as a characterising parameter for fatigue crack propagation. Subsequently, and in order to explain the observed effects of stress ratio, variable amplitude loading, short cracks, etc., the concept of crack closure was introduced based on an effective range of ΔK [5]. Later, other authors questioned the relevance of the crack closure phenomenon, and proposed the conjoint use of two characterising parameters for the driving force: K_{max} and ΔK [6, 7]. More recently, Christopher *et al.* [8] proposed a novel mathematical model (the CJP model) to describe the stress and displacement fields around the tip of a growing fatigue crack, which considers the effects of wake contact and compatibility-induced stresses at the elastic–plastic boundary over the surrounding elastic field. Their model considered characterised the crack tip stress field in terms of a stress intensity component that drives crack growth K_F, and one that retards crack growth, K_R, and the T-stress. Both of these stress intensity components reflect a summation of the relevant force components arising from the applied load, wake contact and compatibility stresses. All of these stress intensity models are, however, based on linear elastic parameters.

However, the use of a stress intensity K parameter is only valid if the crack tip plastic deformation is relatively small, leading to essentially linear elastic overall response of the body, otherwise non-linear parameters must be used. According to the ASTM E647–15 standard [9], the assumption of small-scale yielding (SSY) is valid provided that the following criteria are met for C(T) and M(T) specimens, respectively:

$$(W - a) \geq \frac{4}{\pi}\left(\frac{K_{max}}{Y_0}\right)^2 \tag{1}$$

$$(W - 2a) \geq 1.25\left(\frac{F_{max}}{tY_0}\right)^2 \quad (2)$$

where K_{max} is the maximum stress intensity factor, F_{max} is the maximum force, W is the width of specimen in the direction of crack growth, t is the thickness of specimen, a is the crack length and Y_0 the yield stress of the material. This criterion indicates that the uncracked ligament of the specimen must be relatively large compared with crack and local plasticity dimensions, in order to achieve SSY conditions.

In previous work [10] the authors proposed a procedure to define the boundary of the SSY regime based on crack tip opening displacement (CTOD). The CTOD was predicted numerically, using the finite element method, and compared with the experimental values obtained using a DIC technique. In both cases, a plot of CTOD versus load could be obtained, from which the elastic and plastic CTOD ranges, $\Delta\delta_e$ and $\Delta\delta_p$, respectively, were extracted [11]. The SSY regime was proposed to occur when $\Delta\delta_p/\Delta\delta_e \leq 33\%$, which is equivalent to $\Delta\delta_e/\Delta\delta_t \geq 75\%$, where $\Delta\delta_t = \Delta\delta_e+\Delta\delta_p$ is the total CTOD range [10]. This approach is applied in the present paper to notched samples with various notch radii in order to study its influence on the limitations of SSY. The notched geometries were studied using the finite element method and the analysis included consideration of the effects of plasticity induced crack closure, crack tip blunting, material hardening and residual stresses.

NUMERICAL MODEL

A parametric study was performed on SENT (Single Edge Notch Tension) specimens with four notch geometries and using material parameters that simulated three different aluminium alloys. The effects of notch radius, stress state, hardening behaviour and crack closure on the validity of an SSY assumption have been explored. The constitutive modelling of the alloys 6082-T6 and 7050-T6 utilised kinematic hardening, while the 7050-T6 alloy was also modelled assuming isotropic hardening.

The mechanical behaviour of the materials was assumed to be elastic-plastic. The isotropic elastic domain was defined by the generalized Hooke's law elastic parameters: Young's modulus (E) and Poisson's ratio (ν). The plastic behaviour was described with the von Mises yield criterion coupled with a mixed hardening model using the Voce isotropic and Armstrong-Frederick kinematic hardening laws, under an associated flow rule. Voce isotropic hardening law [12] is given by:

$$Y(\bar{\varepsilon}^p)=Y_0+(Y_{Sat}-Y_0)[1-exp(-C_Y\bar{\varepsilon}^p)] \quad (3)$$

where $Y(\bar{\varepsilon}^p)$ is the flow stress, Y_0, Y_{Sat}, and C_Y are the material parameters of Voce law and $\bar{\varepsilon}^p$ is the equivalent plastic strain. The Armstrong-Frederick kinematic hardening law [13] can be written:

$$\dot{\boldsymbol{X}}=C_X\left[\frac{X_{sat}}{\bar{\sigma}}(\boldsymbol{\sigma}'-\boldsymbol{X})-\boldsymbol{X}\right]\dot{\bar{\varepsilon}}^p \quad (4)$$

where C_X and X_{Sat} are the material parameters, $\bar{\sigma}$ is the equivalent stress, $\boldsymbol{\sigma}'$is the deviatoric Cauchy stress tensor**,** $\boldsymbol{X}$ is the back-stress tensor and $\dot{\bar{\varepsilon}}^p$ is the equivalent plastic strain rate. The material properties can be found in Table 1.

FCGR was simulated in SENT specimens (details given in Figure 1a), with a thickness of 0.1 mm. Only ¼ of the specimen was modelled, see Figure 1b, with the application of appropriate boundary conditions. Note that along the thickness there is also a symmetry condition. The lower right corner is fixed along the horizontal direction, to avoid rigid body movement. Four notch radii, r, were considered: r = 1, 2, 4 and 8 mm (Figures 1d, 1e, 1f and 1g, respectively), whilst maintaining a constant notch depth of 8 mm. A mesh containing 7175 3D linear 8-node hexahedral elements and 7359 nodes was used for the model (Figure 1c). Near the crack tip, mesh elements are 8 × 8 μm and an initial crack increment of 96 μm at the notch root was simulated, representing a distance of 12 mesh elements and approximating a through-thickness notch root crack of the same depth as the specimen thickness. Hence the total initial crack length was a_0 = 8.096 mm.

The crack tip nodes were released at minimum load after two load cycles had been applied. The simulation ended after a crack growth of 159 crack increments, i.e. Δa = 1.272 mm. The loading parameters are presented in Table 2. The maximum nominal stress, σ_{nom}, was measured at the crack tip, at the initiation of the simulation, i.e. for a_0 = 8.096 mm. As it is reflects traction loading, σ_{nom} is given by the ratio between the maximum load, F_{max}, and the cross-sectional area immediately ahead of the tip. An increase in crack length reduces the load-carrying area and consequently increases σ_{nom}. In all simulation cases σ_{nom} was taken as equal to 95.46 MPa. Table 2 also shows the ratio between σ_{nom} and Y_0, i.e., 0.227 and 0.400 for the AA7050-T6 and AA6082-T6 alloys, respectively. Simulations were conducted with and without contact at the crack flanks, to investigate any contribution from crack flank contact on FCGR. In order to provide a reference condition for comparative purposes, an unnotched tension-cracked model was also created. Figure 2 schematically illustrates the four cases simulated.

Table 1. Material properties with isotropic hardening fitted with Voce law.

Material	**Hooke's law**		**Isotropic hardening (Voce)**			**Kinematic Hardening (Armstrong-Frederick)**	
	E [GPa]	v [-]	Y_0 [MPa]	Y_{Sat} [MPa]	C_Y [-]	C_X [-]	X_{Sat} [MPa]
AA7050-T6 kinematic [14]	69.724	0.30	420.5	420.5	3.806	228.91	198.35
AA7050-T6 isotropic	69.724	0.30	420.5	420.5	3.806	0	0
AA6082-T6 [15]	70	0.29	238.15	487.52	0	244.44	83.18

Table 2. Loading parameters for notched-cracked specimens.

Material	***R***	F_{min} **(N)**	F_{max} **(N)**	σ_{nom}/Y_0	***NLC***	**Stress State**
7050-T6 kinematic	0.01	4	400	0.227	2	Plane strain; Plane Stress
7050-T6 Isotropic	0.01	4	400	0.227	2	Plane strain; Plane Stress
6082-T6	0.01	4	400	0.400	2	Plane strain; Plane Stress

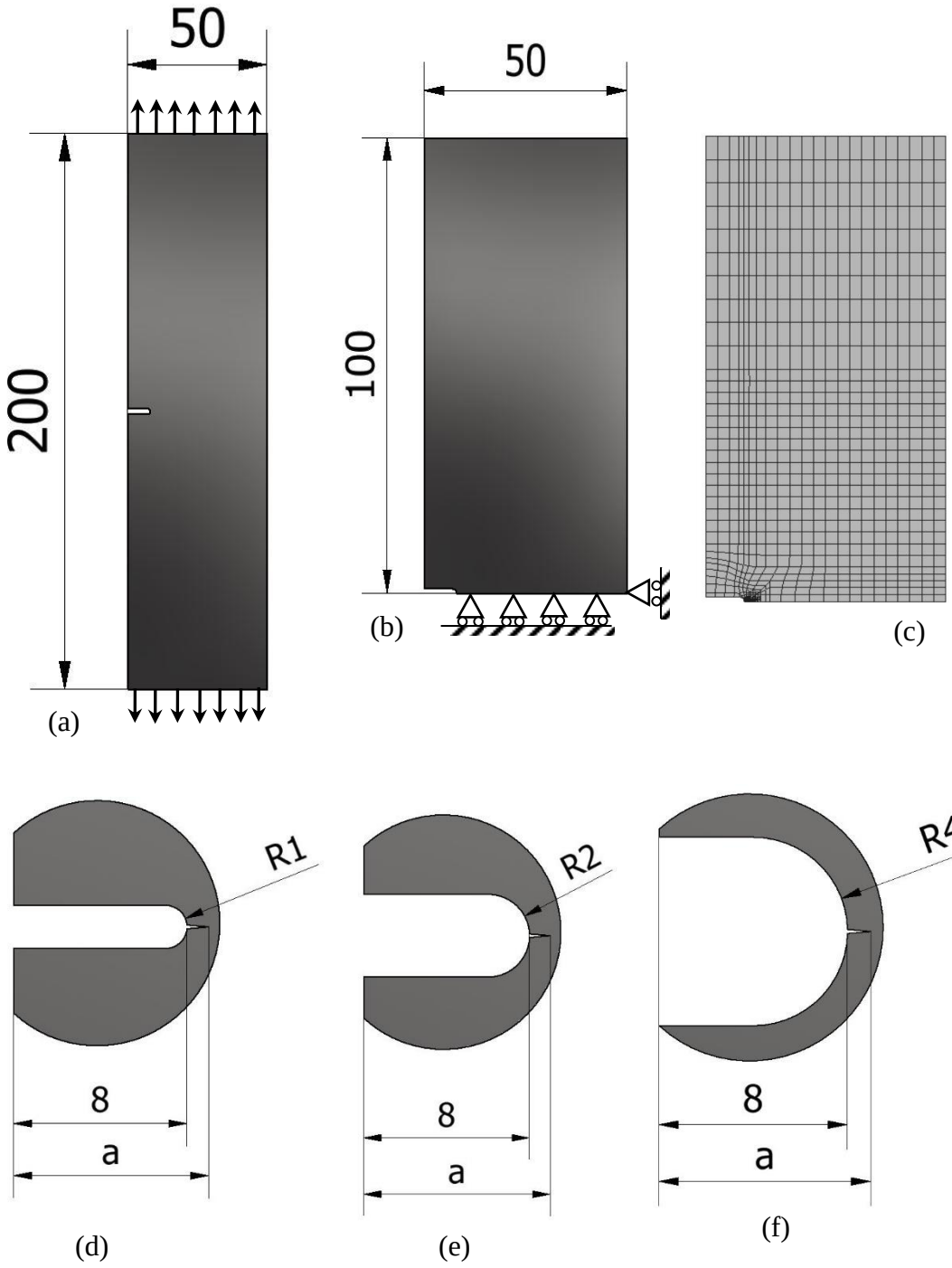

Figure 1. SENT specimen (a) Main dimensions. (b) Boundary conditions. (c) Finite element mesh.
(d) r =1 mm (e) r =2 mm (f) r =4 mm (g) r =8 mm.

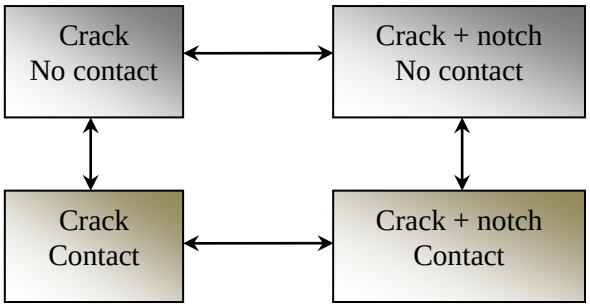

Figure 2**.** Schematic showing the four conditions studied.

The CTOD was measured at the first node behind the crack tip, i.e. at a distance of 8 μm. Figure 3 presents a typical curve of CTOD versus applied load. At minimum load (*A*) the crack is closed, i.e., there is no CTOD at the first node behind crack tip. An increase of load opens the crack at point *B*. After opening, there is a linear region (*B*-*C*) linked to the elastic behaviour of the alloy. Plastic deformation commences after point *C*, and steadily increases up to the maximum load (*D*). The elastic CTOD is obtained by extrapolating to the maximum load the elastic behaviour defined between points C and D (illustrated by the solid line); the plastic CTOD is then obtained by subtracting the elastic CTOD from the total CTOD, and increases non-linearly with load increment. The elastic and plastic CTOD ranges, $\Delta\delta_e$ and $\Delta\delta_p$ respectively, are indicated in Figure 3.

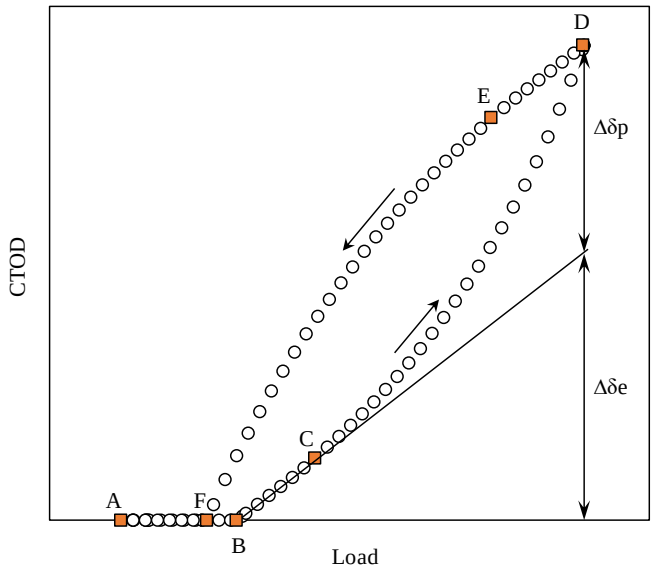

Figure 3. Typical plot of CTOD versus applied load.

The elastic and total CTOD ranges, $\Delta\delta_e$ and $\Delta\delta_t$, respectively, were used to define the parameter $\%\Delta\delta_e$ in equation 5:

$$\%\Delta\delta_e = \frac{\Delta\delta_e}{\Delta\delta_t} \times 100 \quad (5)$$

This parameter has a value of 100% when the CTOD is totally elastic and a value of zero if it was totally plastic. It is therefore an appropriate parameter to study the transition from SSY to LSY. A similar approach has been used by Escalero *et al.* [16], who calculated values of J-integral for elastic and elastic-plastic models of a 42CrMo4 steel and plotted them versus crack length. The boundary of SSY was defined as the point where the two curves started to separate. A difference of 2% was assumed as the criterion for identifying this boundary.

RESULTS

Figures 4a (plane strain) and 4b (plane stress) show the trends in $\Delta\delta_e/\Delta\delta_t$ versus Δa for the alloys 6082-T6 and 7050-T6 undergoing pure kinematic hardening behaviour, for a condition of no crack flank contact. An additional curve shows the data obtained with an assumption of pure isotropic hardening in the case of the 7050-T6 alloy. For a constant value of maximum applied load, as crack length increases $\Delta\delta_e/\Delta\delta_t$ decreases due to the higher levels of plastic deformation that occur at the crack tip. This reflects the fact that longer cracks have higher stress intensity values at the crack tip. Reference [10] proposed that SSY was valid for a value of $\%\Delta\delta_e > 75\%$ and that LSY conditions dominated when $\%\Delta\delta_e < 60\%$. Applying these criteria in the present case of notched specimens indicates that both the 6082-T6 and the 7050-T6 with isotropic hardening lie in the LSY regime while the 7050-T6 with kinematic hardening behaviour lies in the transition region between SSY and LSY. The lower value of yield stress of the 6082-T6 alloy (Table 1) gives higher values of plastic deformation at a given maximum applied load. In the case of the 7050-T6 alloy, pure kinematic behaviour leads to greater hardening in uniaxial tension, than isotropic hardening, offering greater resistance to plastic deformation. The state stress had no influence on $\Delta\delta_e/\Delta\delta_t$ when crack closure is disabled in the model.

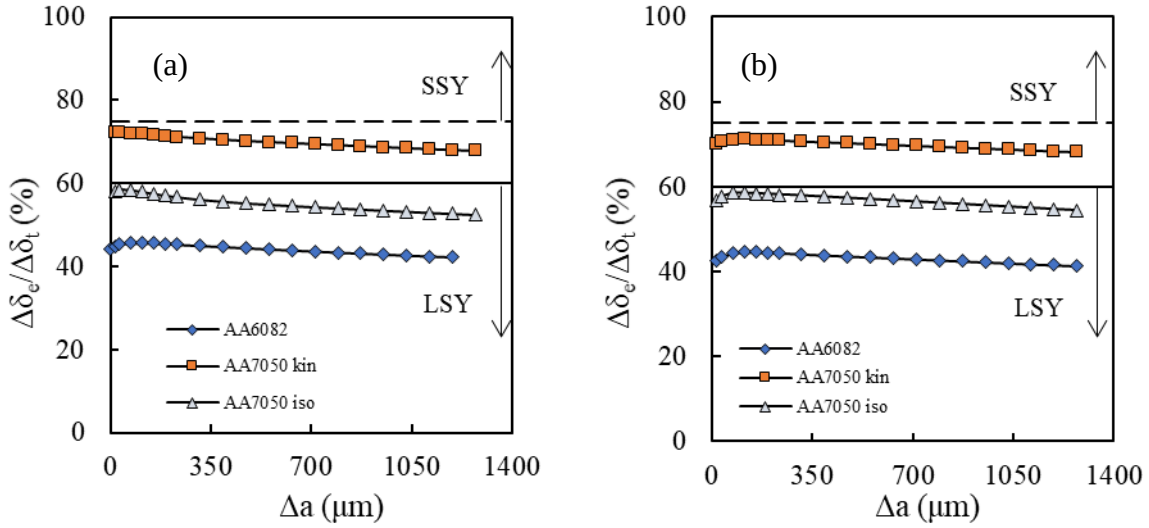

Figure 4. Effect of Δa on SSY/LSY regimes (unnotched specimen; R=0.01; F_{max}=400N; F_{min}=4N; no contact at the crack flanks). (a) Plane Strain; (b) Plane Stress.

Figure 5 shows $\%\Delta\delta_e$ versus Δa data for the three aluminium alloy conditions in the presence of simulated crack closure. The contact of crack flanks is modelled by considering a rigid surface at the symmetry plane, which prevents overlapping of crack surfaces during unloading. Under plane strain conditions, as shown in Figures 5a, 5c and 5e, allowing contact between the crack flanks in the model produces virtually no effect on $\Delta\delta_e/\Delta\delta_t$. Under plane stress conditions, however, (Figures 5b, 5d and 5f) contact between the crack flanks reduces $\Delta\delta_p$ and consequently increases $\Delta\delta_e/\Delta\delta_t$. This phenomenon reflects the overall reduction in the effective load range which reduces the level of plastic deformation at the crack tip.

Figure 6 presents the results of the numerical simulations of crack growth in notched specimens for all four cases with different root radii, r. These results are for the case of no crack flank contact and the equivalent unnotched data from Figures 4a and 4b are also included for comparative purposes. The local stress concentration effect of a notch reduces the plastic component of crack tip displacement, $\Delta\delta_p$, and consequently increases $\Delta\delta_e/\Delta\delta_t$. This effect is more pronounced for higher values of r due to the inverse proportionality observed between notch root radius and the associated stress concentration factor which gives an increased stress triaxiality in the notch root region. The effect of crack length is now more

pronounced, because this parameter also affects the distance to the notch. As Δa increases and the crack tip moves further away from the local stress concentration at the notch root, the values of $\Delta\delta_e/\Delta\delta_t$ found in the notched specimens tend towards the values observed in the unnotched case. The insertion of contact at the fracture surface did not change the observed trends or ranges of $\Delta\delta_e/\Delta\delta_t$ seen in Figure 6. Note that the assumption of SSY is not valid for most of the situations studied.

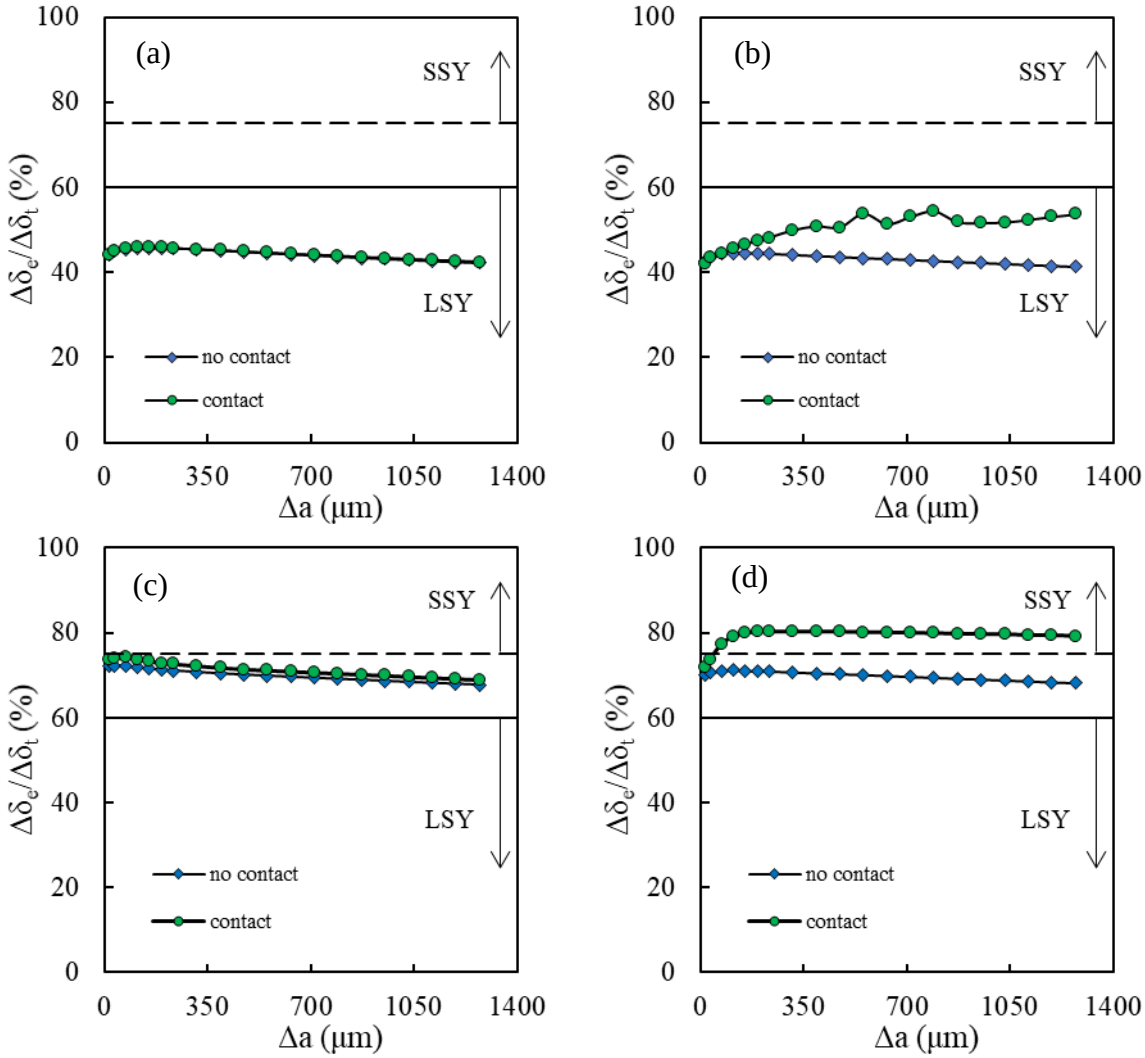

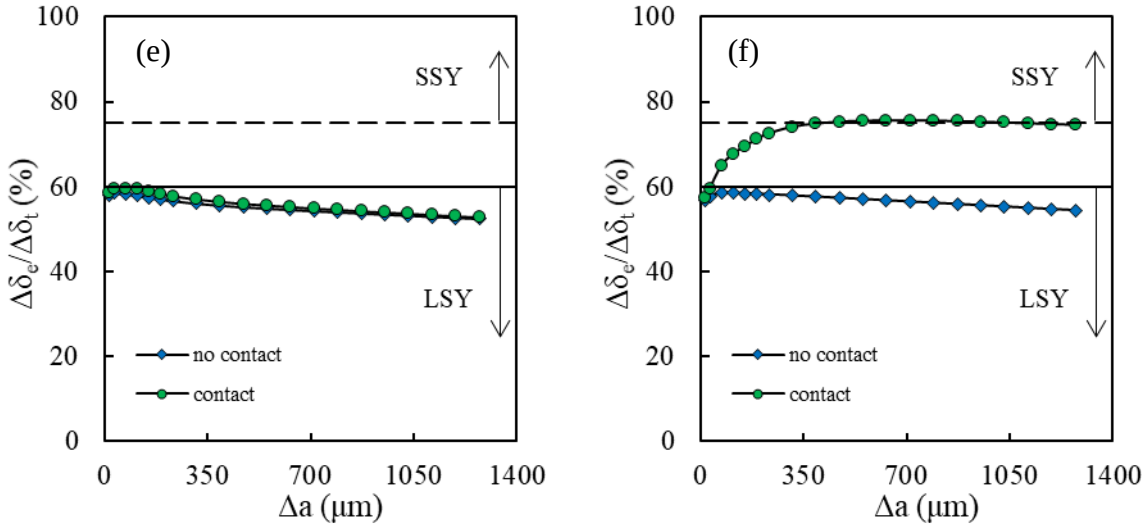

Figure 5. Effect of crack increment, Δa, on the applicability of SSY or LSY, in terms of the ratio $\Delta\delta_e/\Delta\delta_t$ (unnotched specimen; R=0.01; F_{max}=400N; F_{min}=4N). (a) 6082-T6 in plane strain; (b) 6082-T6 in plane stress; (c) 7050-T6 kinematic in plane strain; (d) 7050-T6 kinematic in plane stress; (e) 7050-T6 isotropic in plane strain; (f) 7050-T6 isotropic in plane stress.

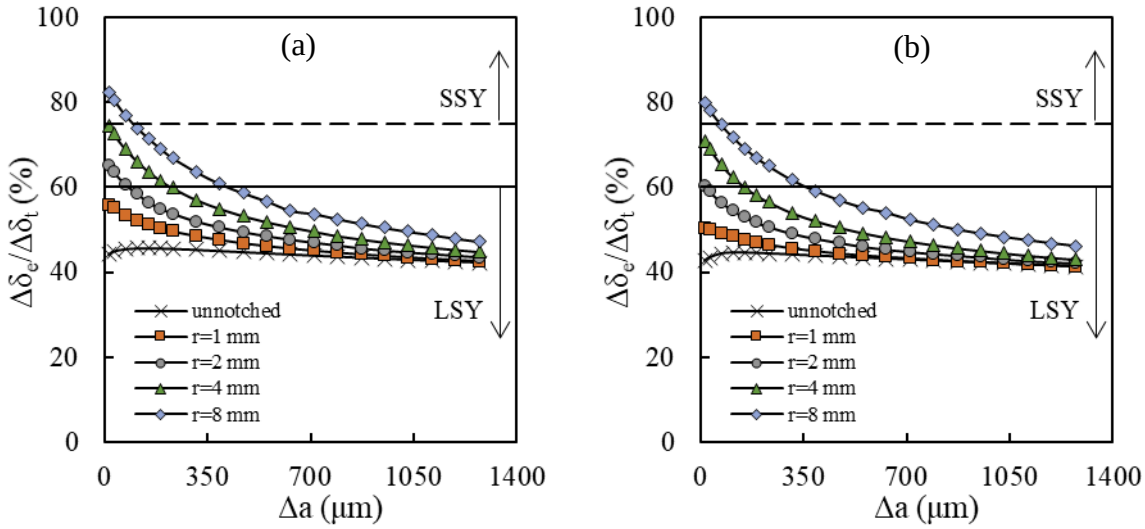

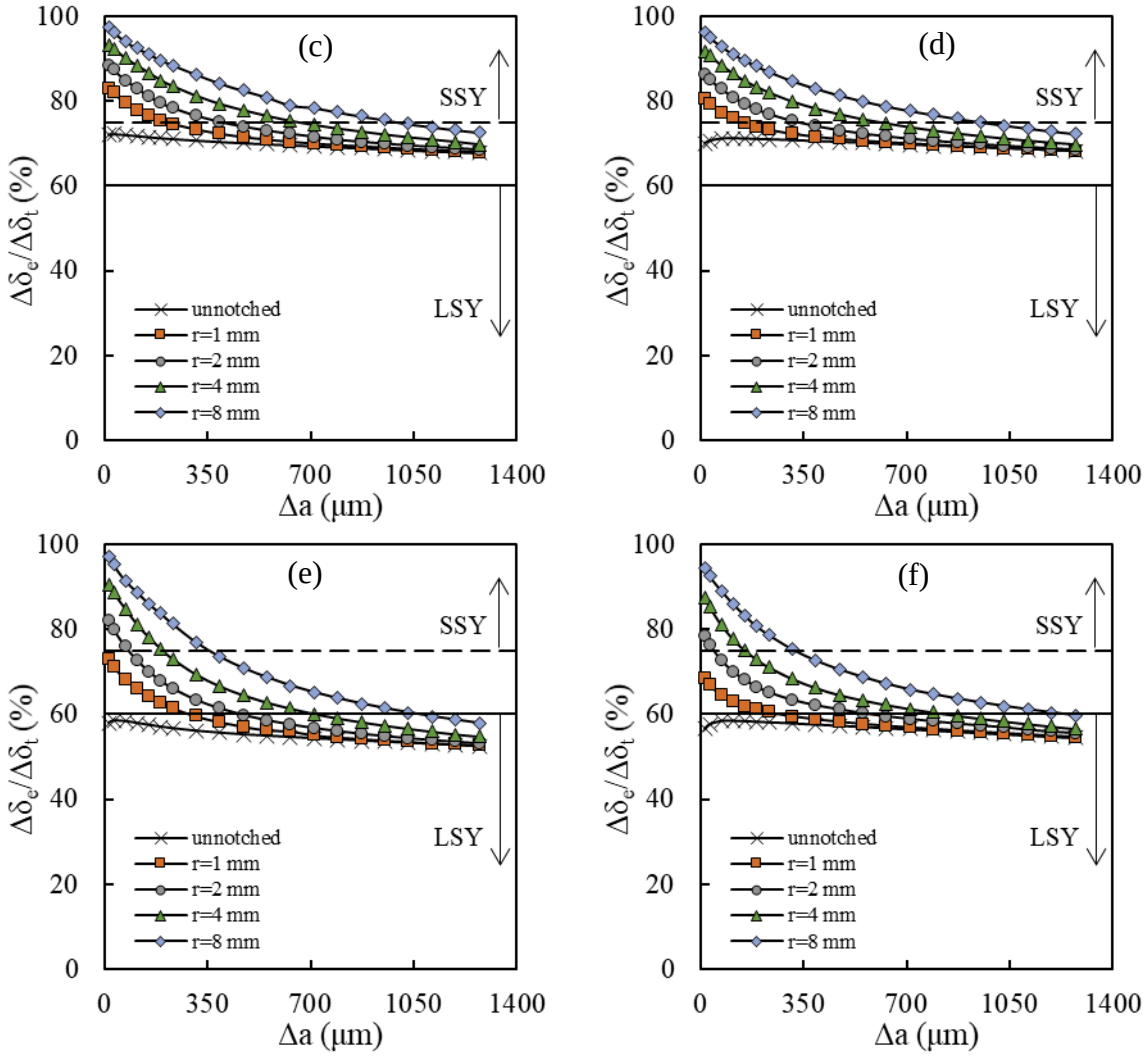

Figure 6. Effect of notch root radius on the transition from SSY to LSY as a function of crack increment Δa (notched specimen; R=0.01; F_{max}=400N; F_{min}=4N; no contact between crack flanks). (a) 6082-T6 in plane strain; (b) 6082-T6 in plane stress; (c) 7050-T6 with kinematic hardening in plane strain; (d) 7050-T6 with kinematic hardening in plane stress; (e) 7050-T6 with isotropic hardening in plane strain; (f) 7050-T6 with isotropic hardening in plane stress.

CONCLUSIONS

The objective in this work was to check the validity of the SSY assumption for notched samples of two aluminium alloys. SSY is a necessary criterion underlying the applicability of linear elastic fracture mechanics (LEFM) to characterising FCGR. The motivation for the work was the fact that although the range of stress intensity factor (ΔK) is widely used to characterise the driving force for fatigue crack propagation, its validity is rarely checked. In a previous work [10] a criterion was proposed to differentiate between SSY and LSY

conditions, based on CTOD and its separation into elastic and plastic components. The small-scale yielding (SSY) regime was proposed to occur when $\%\Delta\delta_e$, the ratio between elastic CTOD, $\Delta\delta_e$, and total CTOD, $\Delta\delta_t$, is greater than 75%, while large-scale yielding (LSY) was proposed to occur when $\%\Delta\delta_e < 60\%$. This criterion has been successfully applied to notched and unnotched SENT specimen geometries in a wide-ranging study that simulated 6082-T6 and 7050-T6 aluminium alloys. Detailed conclusions regarding the influence of notches that can be drawn from the present work include:

1. In unnotched specimens, an increase in crack length promotes a slight progressive decrease in $\%\Delta\delta_e$. The alloy type has a greater effect with the AA6082 more prone to LSY, which is explained by its lower yield stress, compared with AA7050.

2. In unnotched specimens contact between crack flanks increases $\%\Delta\delta_e$ particularly in a plane stress state. The crack closure phenomenon, which is more relevant under plane stress state, reduces the effective load range and therefore the plastic deformation at the crack tip.

3. For notched specimens, an increase in crack length has a more pronounced effect on $\%\Delta\delta_e$. As the crack length increases and the tip moves out of the notch field, and the data for the notched and unnotched cases merge.

4. In notched specimens, an increase of notch radius promotes an increase of $\%\Delta\delta_e$ and promotes the occurrence of SSY.

5. The SSY regime is not observed to be valid in almost all of the notched cases studied. This leads to questions regarding the applicability of LEFM parameters to characterising FCGR.

The work reported in this paper emphasises the importance of checking the applicability of a SSY assumption for any particular combination of specimen geometry, alloy and loading conditions. This can be done, for example, using the criterion proposed in this paper.

Acknowledgements

This research was funded by the project no. 028789, financed by the European Regional Development Fund (FEDER), through the Portugal-2020 program (PT2020), under the Regional Operational Program of the Center (CENTRO-01-0145-FEDER-028789) and the Foundation for Science and Technology IP/MCTES through national funds (PIDDAC). This research is also sponsored by FEDER funds through the program COMPETE – Programa Operacional Factores de Competitividade – and by national funds through FCT – Fundação para a Ciência e a Tecnologia –, under the project UIDB/00285/2020.

References

[1] Forman RG, Kearney VE, Engles RM. (1967) Numerical analysis of crack propagation in cyclic loaded structures. Int J Fracture Mech; 89:459–464.

[2] Erdogan F, Ratwani M. (1970) Fatigue and fracture of cylindrical shells containing circumferential crack. Int J Fracture Mech; 4:379–392.

[3] Kwofie S, Rahbar N. (2011) An equivalent driving force model for crack growth prediction under different stress ratios. Int J Fatigue; 33:1199–1204.

[4] Paris PC, Erdogan J. (1963) Critical analysis of crack growth propagation laws. J Basic Eng; 85D:528–34.

[5] Elber W. The significance of fatigue crack closure under cyclic tension. ASTM STP 1971; 486:230-242.

[6] Vasudevan AK, Sadananda K, Louat N. (1993) Two critical stress intensities for threshold crack propagation. Scripta Metal;28:65–70.

[7] Noroozi AH, Glinka G, Lambert S. (2007) A study of the stress ratio effects on fatigue crack growth using the unified two-parameters fatigue crack growth driving force, Int J Fatigue; 29:1616–1634.

[8] Christopher CJ, James MN, Patterson EA, Tee KF. (2007) Towards a new model of crack tip stress fields. Int J Fract;148:361–371.

[9] ASTM E 647-15. (2015) Standard test method for measurement of fatigue crack growth rates. Philadelphia: American Society for Testing and Materials (ASTM).

[10] Marques B, Borges MF, Antunes FV, Vasco-Olmo JM, Díaz FA, James MN. (2021) Limitations of SSY for fatigue crack growth, Engineering Fracture mechanics, submitted

[11] Marques B, Neto DM, Antunes FV, Vasco-Olmo JM, Díaz FA. (2020) Numerical tool for the analysis of CTOD curves obtained by DIC or FEM. Fat Fract Eng Mater Struct;43:2984–2997.

[12] Voce E. (1948) The Relationship Between Stress and Strain for Homogeneous Deformation. J Inst Met;74:537–562.

[13] Frederick CO, Armstrong PJ. A mathematical representation of the multiaxial Bauschinger effect. Mater High Temp 2007;24:1–26.

[14] Antunes FV, Branco R, Prates PA, Borrego L. (2017) Fatigue crack growth modelling based on CTOD for the 7050-T6 alloy. Fat Fract Eng Mater Struct;40(8):1309–1320.

[15] Antunes FV, Rodrigues SM, Branco R, Camas D. (2016) A numerical analysis of CTOD in constant amplitude fatigue crack growth. Theor Appl Fract Mech;85:45–55.

[16] Escalero M, Muniz-Calvente M, Zabal H, Urrestia I. (2020) Suitability of constraint and closure models for predicting crack growth in generic configurations. Eng Fract Mech;225:106808.